Synthesis, Structure, and Properties of the Organic Conductor $(BEDT\text{-}TTF)_2Br_2SeCN$

Urs Geiser,* H. Hau Wang,* John A. Schlueter, Jack M. Williams,* James L. Smart, Alan C. Cooper, S. Kalyan Kumar, Maria Caleca, James D. Dudek, and K. Douglas Carlson*

Chemistry and Materials Science Divisions, Argonne National Laboratory, Argonne, Illinois 60439

J. Ren and M.-H. Whangbo*

Department of Chemistry, North Carolina State University, Raleigh, North Carolina 27650-8204

J. E. Schirber and W. R. Bayless

Sandia National Laboratories, Albuquerque, New Mexico 87185

Received March 28, 1994[⊗]

A new salt of the electron-donor molecule BEDT-TTF [bis(ethylenedithio)tetrathiafulvalene, or ET] with the unusual "T"-shaped anion Br_2SeCN^- was synthesized. Its crystal structure (space group $P1$, $Z = 1$; $a = 5.9304(6)$ Å, $b = 8.8042(9)$ Å, $c = 16.509(2)$ Å, $\alpha = 95.723(8)°$, $\beta = 98.767(8)°$, $\gamma = 92.192(8)°$, $V = 846.4(2)$Å^3 at 298 K; $a = 5.8131(12)$ Å, $b = 8.666(2)$ Å, $c = 16.626(4)$ Å, $\alpha = 93.75(2)°$, $\beta = 100.62(2)°$, $\gamma = 89.75(2)°$, $V = 821.4(3)$ Å^3 at 122 K) contains layers of ET molecules interspersed with anion layers. A crystallographic phase transition at ~150 K is observed, accompanied by a discontinuity in unit cell angles. The band electronic structure calculation suggests the possibility of one-dimensional conduction, but electron localization renders the system semiconducting over the entire temperature range studied. Inductive techniques showed no sign of superconductivity at temperatures above 1.2 K and pressures below 5 kbar.

Introduction

The electron-donor molecule BEDT-TTF [bis(ethylenedithio)-tetrathiafulvalene, or ET] has been used extensively in the preparation of charge transfer salts. This donor molecule has been combined with anions of various compositions and geometries, including linear, tetrahedral, octahedral, monoatomic, and polymeric. These complexes exhibit a wide range of electrical properties ranging from semiconductive to metallic. Several compounds undergo transitions to a superconductive state at low temperatures.[1]

All organic superconductors with critical temperatures above 10 K contain polymeric anions and a κ-phase structure. κ-$(ET)_2Cu[N(CN)_2]Br$ (T_c = 11.6 K)[2], κ-$(ET)_2Cu[N(CN)_2]Cl$ (T_c = 12.8 K at 0.3 kbar)[3], and κ-$(ET)_2Cu(NCS)_2$ (T_c = 10.4 K)[4-6] all contain copper(I) complex anions with various halide or pseudohalide ligands. In an attempt to synthesize new derivatives of these anions, we combined CuBr with selenocyanate. Instead of a salt of the expected $Cu(SeCN)Br^-$ complex anion, oxidation of the selenocyanate group to Br_2SeCN^- occurred. In this paper, we report the synthesis, electrocrystallization, crystal structure, electrical conductivity, ESR properties, and the band electronic structure of the first ET salt to contain this uncommon, "T"-shaped anion.

Experimental Section

Synthesis. ET was synthesized following the procedure of Larsen and Lenoir[7] with the following modification: The cyclization step was performed with 30% HBr in acetic acid at room temperature, which yielded ethylenedithio-1,3-dithiole-2-one more efficiently than the reported cyclization with concentrated sulfuric acid. 1,1,2-Trichloroethane (TCE, Aldrich, 98%) was distilled from P_2O_5 and passed through an alumina column prior to use. Absolute ethanol (Midwest Grain Products) was used without further purification. Potassium selenocyanate (Alfa, 95+%) was recrystallized from methanol/diethyl ether prior to use. Elemental analyses were performed at Galbraith Laboratories (Knoxville, TN) or Midwest Microlab (Indianapolis, IN).

(PPN)SeCN. Bis(triphenylphosphoranylidene)ammonium selenocyanate was prepared via a metathesis reaction. KSeCN (4.0 g, 28 mmol) was dissolved in deionized water (20 mL) and gravity filtered. (PPN)Cl (Aldrich, 97%; 15.87 g, 28 mmol) was dissolved in deionized water (2 L) and gravity filtered. Combination of these two solutions resulted in a white precipitate, which was collected by suction filtration. This crude product was recrystallized from acetonitrile/diethyl ether and dried under vacuum.

Anal. Calcd for $C_{37}H_{30}N_2P_2Se$: C, 69.05; H, 4.70; N, 4.35; P, 9.63; Se, 12.27. Found: C, 68.58; H, 4.63; N, 3.93. Infrared spectroscopy: ν_{CN} = 2064 cm^{-1}. Mp: 199−200 °C.

(Ph_4P)SeCN. Tetraphenylphosphonium selenocyanate was prepared in the same manner. KSeCN (4.0 g, 28 mmol) was dissolved in

* Authors to whom correspondence is to be addressed.

[⊗] Abstract published in *Advance ACS Abstracts,* October 1, 1994.

(1) Williams, J. M.; Ferraro, J. R.; Thorn, R. J.; Carlson, K. D.; Geiser, U.; Wang, H. H.; Kini, A. M.; Whangbo, M.-H. *Organic Superconductors (Including Fullerenes): Synthesis, Structure, Properties and Theory*; Prentice Hall: Englewood Cliffs, New Jersey, 1992.

(2) Kini, A. M.; Geiser, U.; Wang, H. H.; Carlson, K. D.; Williams, J. M.; Kwok, W. K.; Vandervoort, K. G.; Thompson, J. E.; Stupka, D. L.; Jung, D.; Whangbo, M.-H. *Inorg. Chem.* **1990**, *29*, 2555.

(3) Williams, J. M.; Kini, A. M.; Wang, H. H.; Carlson, K. D.; Geiser, U.; Montgomery, L. K.; Pyrka, G. J.; Watkins, D. M.; Kommers, J. M.; Boryschuk, S. J.; Strieby Crouch, A. V.; Kwok, W. K.; Schirber, J. E.; Overmyer, D. L.; Jung, D.; Whangbo, M.-H. *Inorg. Chem.* **1990**, *29*, 3262.

(4) Urayama, H.; Yamochi, H.; Saito, G.; Nozawa, K.; Sugano, T.; Kinoshita, M.; Sato, S.; Oshima, K.; Kawamoto, A.; Tanaka, J. *Chem. Lett.* **1988**, *55*.

(5) Gärtner, S.; Gogu, E.; Heinen, I.; Keller, H. J.; Klutz, T.; Schweitzer, D. *Solid State Commun.* **1988**, *65*, 1531.

(6) Carlson, K. D.; Geiser, U.; Kini, A. M.; Wang, H. H.; Montgomery, L. K.; Kwok, W. K.; Beno, M. A.; Williams, J. M.; Cariss, C. S.; Crabtree, G. W.; Whangbo, M.-H.; Evain, M. *Inorg. Chem.* **1988**, *27*, 965.

(7) Larsen, J.; Lenoir, C. *Synthesis* **1989**, 134.

0020-1669/94/1333-5101$04.50/0

deionized water (25 mL) and gravity filtered. $(Ph_4P)Br$ (Aldrich, 97%; 11.74 g, 28 mmol) was dissolved in deionized water (750 mL) and gravity filtered. Combination of these two solutions resulted in a white precipitate, which was collected by suction filtration. This crude product was recrystallized from acetonitrile/diethyl ether and dried under vacuum.

Anal. Calcd for $C_{25}H_{20}NPSe$: C, 67.57; H, 4.54; N, 3.15; P, 6.97; Se, 17.77. Found: C, 67.54; H, 4.53; N, 3.23. Infrared spectroscopy: $\nu_{CN} = 2064$ cm^{-1}. Mp: 295−297 °C.

$(PhMe_3N)SeCN$. Phenyltrimethylammonium selenocyanate was prepared according to the published procedure.[8] KSeCN (4.90 g, 34 mmol) was dissolved in 20 mL of methanol. To this solution was added $(PhMe_3N)Br$ (Aldrich, 7.35 g, 34 mmol). The white KBr precipitate was removed by gravity filtration after stirring 20 min. Diethyl ether (200 mL) was added to precipitate the product as white crystals (yield: 7.81 g; 95%). The salt was recrystallized from acetone/diethyl ether.

Anal. Calcd for $C_{10}H_{14}N_2Se$: C, 49.80; H, 5.85; N, 11.61; Se, 32.74. Found: C, 49.69; H, 5.71; N, 11.41. Infrared spectroscopy: $\nu_{CN} = 2056$ cm^{-1}. Mp: 118−121 °C.

$(PhMe_3N)Br_2SeCN$. Phenyltrimethylammonium dibromoselenocyanate was prepared according to the published procedure.[8] $(PhMe_3N)SeCN$ (5.0 g, 20.75 mmol) was dissolved in methylene chloride (20 mL). A 10% (v/v) solution of bromine in methylene chloride (5.40 mL, 20.75 mmol) was added. This solution was cooled to ~5 °C for 30 min, at which time methylene chloride (150 mL) and diethyl ether (10 mL) were added. After this mixture was warmed to ~30 °C, a bright red, uncharacterized precipitate was removed by suction filtration. The filtrate was slowly cooled to −5 °C, which precipitated yellow crystals. These crystals were recrystallized from methylene chloride (100 mL) and dried under vacuum (yield: 4.3 g; 52%).

Anal. Calcd for $C_{10}H_{14}N_2Br_2Se$: C, 29.95; H, 3.53; N, 6.98; Br, 39.85; Se, 19.69. Found: C, 29.93; H, 3.52; N, 6.94; Br, 39.82. Infrared spectroscopy: $\nu_{CN} = 2139$ cm^{-1}. Mp: 92−93 °C.

Single Crystals of $(ET)_2Br_2SeCN$. Single crystals of the title compound were grown at 23 °C by standard electrocrystallization techniques.[9] The electrochemical cell was assembled in an argon-filled drybox. $(PhMe_3N)SeCN$ (51.1 mg, 0.21 mmol) and CuBr (30.0 mg, 0.21 mmol)[10] were dissolved in 10 mL of a 9:1 (v/v) TCE/EtOH solution and divided between the two chambers of an H-cell. Pt electrodes were employed. ET (8.2 mg, 0.021 mmol) was dissolved in 5 mL of 9:1 (v/v) TCE/EtOH and added to the anode chamber. A current density of 0.2 μA/cm^2 was initially applied and gradually increased over a period of 1 month to 3.8 μA/cm^2, at which time crystallization of black needles commenced not at the anode surface but on the glass wall of the anode compartment. Crystals were left to grow for a period of 7 days. The title compound is characterized by rod-shaped crystals, whereas a small portion of the product consists of small, thin intergrown plates of a different, not yet fully characterized phase.

Polycrystalline $(ET)_2Br_2SeCN$. ET (50.1 mg, 0.13 mmol) was dissolved in 25 mL of 9:1 (v/v) TCE/EtOH. $(PhMe_3N)Br_2SeCN$ (300.8 mg, 0.75 mmol) was dissolved in 25 mL of 9:1 (v/v) TCE/EtOH. These two solutions were gravity filtered and mixed under stirring. The black precipitate which formed was collected by suction filtration, washed with TCE, and dried under vacuum (yield: 50.14 mg; 75%).

Anal. Calcd for $C_{21}H_{16}NBr_2S_{16}Se$: C, 24.39; H, 1.56; N, 1.36; Br, 15.45; S, 49.61; Se, 7.64. Found: C, 24.30; H, 1.50; N, 1.24; Br, 14.98; Se, 7.47.

X-ray Diffraction. The single-crystal X-ray diffraction experiments were carried out on a computer-controlled modified Syntex $P2_1$ four-circle diffractometer. Low temperatures were achieved by use of a regulated cold nitrogen flow attachment. The temperature was measured by use of a thermocouple positioned in the cold gas stream near the sample. Unit cell data were obtained from the angle settings of 21−45 carefully centered reflections with $19° < 2\theta < 39°$. All intensity data were corrected for Lorentz, polarization, and absorption effects (Gaussian integration method using the measured sample shape and size). Further details are given in Table 1 and in the supplementary material. The computer programs used were part of the *UCLA Crystallographic Package*.[11] Standard sources for the atomic scattering factors, including anomalous dispersion corrections, were employed.[12] Powder X-ray diffraction patterns of the polycrystalline products were obtained on a Norelco powder diffractometer.

Table 1. Crystallographic Data for $(ET)_2Br_2SeCN$ at 298 K and 122 K, Respectively

$C_{21}H_{16}Br_2NS_{16}Se$	fw 1034.09
$a = 5.9304(6), 5.8131(12)$ Å	space group: $P\bar{1}$ (No. 1)
$b = 8.8042(9), 8.666(2)$ Å	$T = 298, 122$ K
$c = 16.509(2), 16.626(4)$ Å	$\lambda = 0.7107$ Å
$\alpha = 95.723(8), 93.75(2)°$	$\varrho_{calcd} = 2.029, 2.089$ g cm^{-3}
$\beta = 98.767(8), 100.62(2)°$	$\mu = 44.06, 45.38$ cm^{-1}
$\gamma = 92.192(8), 89.75(2)°$	$R(F_o)^a = 0.041, 0.040$
$V = 846.4(2), 821.4(3)$ Å^3	$R_w(F_o)^b = 0.042, 0.035$
$Z = 1$	

$^a R(F_0) = \sum||F_o| - |F_c||/\sum|F_o|$. $^b R_w(F_o) = [\sum w(|F_o| - |F_c|)^2/\sum wF_o^2]^{1/2}$.

Physical Measurements. Measurements of the temperature dependence of the electrical conductivity were carried out by use of the conventional four-probe technique. Gold wire (0.0005 in. diameter), secured along the needle axis of the crystals with silver conducting paste, served as the current and voltage contacts. Crystals were cooled at a rate of 6° min^{-1}. Magnetic susceptibilities were measured on a Lake Shore Model 7121 ac susceptometer by use of a modulation frequency of 111 Hz.

An rf impedance technique described earlier[13] was also used to detect superconductivity. In this apparatus hydrostatic pressure up to 5 kbar was generated in freezing helium.[14] A small chip of pure Nb was affixed to the rf coil to provide an internal pressure-independent thermometer and to check the sensitivity of the measurements.

ESR spectra were recorded on an IBM ER-200 X-band spectrometer equipped with a TE_{102} microwave cavity and an Oxford EPR-900 flow cryostat with an ITC4 temperature controller. Single crystals were mounted at the end of a quartz rod which could be rotated perpendicular to the field by use of a goniometer.

Results

Crystal Structure of $(ET)_2Br_2SeCN$. The room temperature crystal structure of $(ET)_2Br_2SeCN$ was initially solved by direct methods in the centrosymmetric space group $P\bar{1}$. A linear, triatomic unit located at the origin was assigned as a $CuBr_2^-$ anion, and the ET molecules were observed in subsequent difference Fourier maps. However, the "Cu"−Br bond distance was too long by 0.2 Å for such a species, and further peaks the size of first-row elements were found in the difference maps at x, 0, 0 ($x \approx 0.3$ and 0.5). These peaks were assigned to a disordered C−N group, and the "Cu" atom at the origin was reassigned as selenium. From this point, two parallel refinements were carried out, one in the centrosymmetric space group with a disordered anion, and the other in the noncentrosymmetric space group $P1$ with an ordered model. It should be noted that the non-bonded Se···N distance between neighboring anions and the next-nearest-neighbor intramolecular Se···N distance are each approximately equal to half the a-axis repeat distance. Therefore, the only atom breaking the symmetry is the anion-carbon atom. In the noncentrosymmetric model, large correlations were observed between corresponding atomic parameters of the now nonequivalent ET molecules. Although both

(8) Hauge, S.; Marøy, K. *Acta. Chem. Scand.* **1992**, *46*, 1166.
(9) Emge, T. J.; Wang, H. H.; Beno, M. A.; Williams, J. M.; Whangbo, M.-H.; Evain, M. *J. Am. Chem. Soc.* **1986**, *108*, 8215.
(10) Originally, a copper complex anion with mixed bromide and selenocyanate ligands was expected to form.
(11) Strouse, C. *UCLA Crystallographic Package*; University of California, Los Angeles, CA, 1985.
(12) *International Tables for X-ray Crystallography*; Kynoch Press: Birmingham, England, 1974.
(13) Azevedo, L. J.; Schirber, J. E.; Williams, J. M.; Beno, M. A.; Stephens, D. R. *Phys. Rev. B: Condens. Matter* **1984**, *30*, 1570.
(14) Schirber, J. E. *Cryogenics* **1970**, *10*, 418.

Table 2. Atomic Coordinates and Equivalent Isotropic Thermal Parameters for (ET)$_2$Br$_2$SeCN[a]

	x	y	z	10^4U_{eq}	occupancy		x	y	z	10^4U_{eq}	occupancy
Se	0.0000	0.0000	0.0000	435(2)	1.0000	C9A (RT)	0.596(3)	0.323(2)	0.1228(12)	280(32)*	0.414(18)
	0.0000	0.0000	0.0000	297(2)	1.0000	C9B (RT)	0.526(3)	0.417(2)	0.1204(12)	280*	0.586[†]
Br1	−0.0013(5)	0.2779(3)	−0.0381(2)	531(6)	1.0000	C9 (122 K)	0.535(3)	0.352(2)	0.1150(8)	206(25)	1.0000
	−0.0526(6)	0.2868(3)	−0.0316(2)	252(4)	1.0000	C10A (RT)	0.770(5)	0.451(5)	0.149(2)	395(43)*	0.414[†]
Br2	0.0040(5)	−0.2766(4)	0.0360(2)	587(7)	1.0000	C10B (RT)	0.795(3)	0.379(2)	0.1466(12)	395*	0.586[†]
	0.0538(6)	−0.2882(3)	0.0315(2)	162(4)	1.0000	C10 (122 K)	0.683(3)	0.493(2)	0.1443(8)	219(25)	1.0000
N	0.506(4)	−0.012(3)	0.0065(12)	686(38)	1.0000	S11	0.7492(9)	0.8552(6)	0.4811(3)	477(15)	1.0000
	0.4853(14)	0.0210(8)	−0.0059(5)	217(12)*	1.0000		0.7479(8)	0.8586(5)	0.4850(3)	175(9)	1.0000
C0	0.2924(15)	0.0053(11)	−0.0015(5)	481(32)	1.0000	S12	0.3073(8)	0.7020(5)	0.4070(3)	406(14)	1.0000
	0.2891(13)	0.0167(8)	−0.0035(4)	189(18)	1.0000		0.3042(8)	0.7000(5)	0.4113(2)	126(8)	1.0000
S1	0.2623(8)	0.1443(6)	0.5182(3)	465(14)	1.0000	S13	0.6915(8)	0.7477(6)	0.6554(3)	490(15)	1.0000
	0.2640(8)	0.1396(5)	0.5149(2)	146(9)	1.0000		0.7131(7)	0.7406(5)	0.6607(2)	111(8)	1.0000
S2	0.7028(9)	0.3019(6)	0.5904(3)	465(15)	1.0000	S14	0.2415(8)	0.5974(6)	0.5877(3)	398(13)	1.0000
	0.7101(8)	0.2953(5)	0.5873(3)	169(9)	1.0000		0.2559(7)	0.5948(5)	0.5936(2)	111(8)	1.0000
S3	0.3180(8)	0.2527(6)	0.3408(3)	431(14)	1.0000	S15	0.8363(9)	0.9753(7)	0.3290(3)	551(17)	1.0000
	0.2991(9)	0.2583(5)	0.3396(2)	203(10)	1.0000		0.8332(8)	0.9817(5)	0.3322(3)	190(10)	1.0000
S4	0.7638(8)	0.4017(5)	0.4107(3)	412(13)	1.0000	S16	0.3206(10)	0.7814(8)	0.2401(3)	603(19)	1.0000
	0.7563(8)	0.4035(5)	0.4065(2)	182(9)	1.0000		0.3119(8)	0.7751(5)	0.2427(2)	145(9)	1.0000
S5	0.1605(10)	0.0232(7)	0.6681(3)	560(17)	1.0000	S17	0.6753(8)	0.6881(6)	0.8265(3)	481(15)	1.0000
	0.1780(8)	0.0187(5)	0.6674(2)	172(10)	1.0000		0.7167(8)	0.6680(5)	0.8318(2)	146(9)	1.0000
S6	0.6879(9)	0.2144(8)	0.7585(3)	629(20)	1.0000	S18	0.1336(9)	0.5117(6)	0.7446(3)	474(14)	1.0000
	0.6951(8)	0.2232(5)	0.7578(3)	186(10)	1.0000		0.1622(8)	0.5037(5)	0.7522(3)	307(10)	1.0000
S7	0.3318(9)	0.3106(6)	0.1699(3)	505(16)	1.0000	C11	0.515(2)	0.752(2)	0.4970(7)	332(43)	1.0000
	0.2874(8)	0.3342(5)	0.1682(2)	148(9)	1.0000		0.517(2)	0.7501(13)	0.4990(7)	92(21)*	1.0000
S8	0.8686(8)	0.4861(6)	0.2504(3)	506(15)	1.0000	C12	0.478(3)	0.703(2)	0.5665(10)	507(54)	1.0000
	0.8465(8)	0.4969(5)	0.2490(2)	142(9)	1.0000		0.497(2)	0.6959(12)	0.5761(6)	55(19)*	1.0000
C1	0.507(2)	0.255(2)	0.5047(10)	368(45)	1.0000	C13	0.647(3)	0.863(2)	0.3745(10)	461(38)	1.0000
	0.506(2)	0.254(2)	0.4998(8)	166(25)*	1.0000		0.641(2)	0.8725(14)	0.3781(8)	173(25)*	1.0000
C2	0.523(2)	0.2963(14)	0.4255(7)	207(33)	1.0000	C14	0.468(2)	0.7991(14)	0.3415(9)	290(30)*	1.0000
	0.521(2)	0.2946(15)	0.4263(8)	189(26)*	1.0000		0.460(2)	0.7962(13)	0.3468(7)	129(22)*	1.0000
C3	0.348(2)	0.124(2)	0.6200(9)	265(28)*	1.0000	C15	0.544(2)	0.664(2)	0.7254(9)	315(41)	1.0000
	0.353(2)	0.1290(12)	0.6196(6)	73(19)*	1.0000		0.566(2)	0.650(2)	0.7288(9)	242(29)*	1.0000
C4	0.571(2)	0.202(2)	0.6553(10)	453(39)	1.0000	C16	0.331(3)	0.593(2)	0.6908(9)	275(30)*	1.0000
	0.575(2)	0.2014(13)	0.6558(7)	116(21)*	1.0000		0.357(2)	0.5868(14)	0.6981(7)	89(22)*	1.0000
C5	0.477(3)	0.335(2)	0.2741(8)	427(48)	1.0000	C17A (RT)	0.737(5)	0.997(5)	0.231(2)	359(40)*	0.35(3)
	0.436(2)	0.3454(11)	0.2690(6)	18(17)*	1.0000	C17B (RT)	0.758(3)	0.922(3)	0.2246(11)	359*	0.65[†]
C6	0.673(2)	0.397(2)	0.3024(9)	379(34)	1.0000	C17 (122 K)	0.720(2)	0.9253(13)	0.2252(7)	157(23)*	1.0000
	0.649(2)	0.411(2)	0.2991(8)	148(25)*	1.0000	C18	0.502(5)	0.885(4)	0.1922(14)	1369(115)	1.0000
C7A (RT)	0.268(3)	0.123(2)	0.7796(10)	240(31)*	0.531(16)		0.466(3)	0.917(2)	0.1984(9)	171(26)*	1.0000
C7B (RT)	0.315(3)	0.053(3)	0.7765(11)	240*	0.469[†]	C19	0.484(4)	0.592(3)	0.8832(12)	1189(97)	1.0000
C7 (122 K)	0.271(2)	0.0845(12)	0.7738(7)	142(22)*	1.0000		0.465(2)	0.658(2)	0.8798(8)	158(23)*	1.0000
C8A (RT)	0.526(4)	0.090(2)	0.8046(13)	276(32)*	0.531[†]	C20A (RT)	0.306(5)	0.521(3)	0.8491(14)	300(36)*	0.37(3)
C8B (RT)	0.426(3)	0.165(2)	0.8034(13)	276*	0.469[†]	C20B (RT)	0.252(3)	0.599(2)	0.8507(11)	300*	0.63[†]
C8 (122 K)	0.546(3)	0.071(2)	0.7986(8)	182(24)	1.0000	C20 (122 K)	0.327(2)	0.507(2)	0.8555(9)	148(25)*	1.0000

[a] For each atom, the values at room temperature are given on the first line and the values at 122 K on the second line. $U_{eq} = {}^1/_3\sum_{ij}U_{ij}a_i^*a_j^*\mathbf{a}_i\cdot\mathbf{a}_j$. [b] An asterisk denotes a value for an atom refined isotropically. [c] Occ(C8A) = Occ(C7A), Occ(C7B) = Occ(C8B) = 1.000-Occ(C7A); similar for C9, C10, C17, C20.

refinements gave satisfactory results, the noncentrosymmetric model was preferred, based on Hamilton's R value criterion wR (cent)/wR(noncent) = 1.213 > 1.0447 = $\mathcal{R}_{174,2446,0.01}$ (the cutoff criterion at the 1% error level for 174 additional variables and 2446 degrees of freedom).[12] The noncentrosymmetric model also is more realistic, since two adjacent molecules cannot have their C−N groups pointing at each other. However, we cannot exclude the possibility that adjacent anion chains have their polarity reversed at random. Such a structure would be overall centrosymmetric, but non-centrosymmetric on a local level. The statistics of the data do not allow a distinction from the adopted $P1$ model. Because of the almost centric symmetry present, the refinement was hampered by strong correlations among the variables, and several carbon atoms had to be refined with isotropic thermal parameters in order to obtain positive-definite temperature factors. Most of the ethylene-end-group carbon atomic parameters were refined with a split-atom model in order to describe the conformational disorder so often found in ET salts at ambient temperature. Positional parameters are listed in Table 2, and bond lengths and angles in Tables 3 and 4, respectively. The atomic numbering and the molecular geometry of the ET molecule are shown in Figure 1.

A different crystal of the salt was cooled to 122 K, and an intensity data set was collected. The crystal structure at low temperature was basically the same as at room temperature, and the refinement proceeded from room temperature coordinates as a starting point. At the low temperature, the ethylene groups were ordered, and hydrogen atoms fixed at calculated positions ($d_{C\text{-}H}$ = 0.95 Å) were included in the final stages of refinement. The initial positional parameters determined at 122 K are also listed in Table 2, and the bond lengths and angles are given in Tables 3 and 4, respectively.

At both temperatures, the crystal structure of (ET)$_2$Br$_2$SeCN consists of layers of partially oxidized ET radical-cations alternating with anion layers; see Figure 2. These layers form the ab-plane. The two crystallographically independent ET molecules are essentially parallel to each other, as they are related by pseudo-inversion symmetry. The long axis of the donor molecule is approximately perpendicular to the ab-plane, with the central C=C vectors of each molecule forming angles (at 298 K) of 24.1(7) and 30.6(9)°, respectively, with the ab-plane normal, and 15.3(7) and 20.9(9)°, respectively, with the c-axis. The corresponding values at 122 K are 23.9(8)°, 27.6-(6)°, 15.9(8)°, and 19.9(6)°, respectively. Because of the

Table 3. Interatomic Distances (Å) in $(ET)_2Br_2SeCN$[a]

	T = 298 K	T = 122 K		T = 298 K	T = 122 K		T = 298 K	T = 122 K		T = 298 K	T = 122 K
Se−C0	1.737(9)	1.699(7)	S6−C8A	1.73(2)	1.818(13)	S11−C13	1.78(2)	1.784(13)	S18−C20A	1.86(2)	1.805(15)
Se−Br1	2.586(3)	2.579(3)	S6−C8B	1.88(2)		S12−C11	1.785(13)	1.760(12)	S18−C20B	1.83(2)	
Se−Br2	2.564(3)	2.591(3)	S7−C5	1.791(14)	1.735(10)	S12−C14	1.801(13)	1.773(11)	C11−C12	1.31(2)	1.417(14)
N−C0	1.27(2)	1.150(10)	S7−C9A	1.86(2)	1.833(14)	S13−C12	1.79(2)	1.729(11)	C13−C14	1.21(2)	1.25(2)
S1−C1	1.769(14)	1.789(12)	S7−C9B	1.80(2)		S13−C15	1.755(15)	1.763(14)	C15−C16	1.40(2)	1.33(2)
S1−C3	1.708(14)	1.730(11)	S8−C6	1.75(2)	1.736(13)	S14−C12	1.75(2)	1.735(10)	C17A−C18	1.68(4)	1.46(2)
S2−C1	1.69(2)	1.719(14)	S8−C10A	1.68(3)	1.823(14)	S14−C16	1.710(14)	1.734(12)	C17B−C18	1.54(3)	
S2−C4	1.707(14)	1.741(11)	S8−C10B	1.85(2)		S15−C13	1.77(2)	1.775(12)	C19−C20A	1.23(3)	1.53(2)
S3−C2	1.706(12)	1.759(14)	C1−C2	1.41(2)	1.31(2)	S15−C17A	1.66(3)	1.814(12)	C19−C20B	1.40(3)	
S3−C5	1.751(13)	1.746(10)	C3−C4	1.47(2)	1.446(14)	S15−C17B	1.73(2)		Se···N[i]	2.95(2)	2.980(8)
S4−C2	1.737(10)	1.758(12)	C5−C6	1.26(2)	1.36(2)	S16−C14	1.754(14)	1.784(12)	S3···S8[i]	3.657(6)	3.517(5)
S4−C6	1.783(13)	1.785(14)	C7A−C8A	1.57(3)	1.58(2)	S16−C18	1.72(2)	1.796(14)	S7···S8[i]	3.568(7)	3.370(5)
S5−C3	1.730(15)	1.728(11)	C7B−C8B	1.17(3)		S17−C15	1.721(13)	1.772(14)	S3···S15[ii]	3.656(6)	3.604(5)
S5−C7A	1.96(2)	1.806(11)	C9A−C10A	1.49(3)	1.50(2)	S17−C19	1.81(2)	1.795(14)	S5···S13[ii]	3.587(6)	3.610(4)
S5−C7B	1.87(2)		C9B−C10B	1.65(3)		S18−C16	1.747(15)	1.752(12)	S13···S18[iii]	3.645(7)	3.499(5)
S6−C4	1.730(14)	1.709(12)	S11−C11	1.70(2)	1.703(11)				S17···S18[iii]	3.557(7)	3.386(5)

[a] Selected intermolecular contacts shorter than the sum of the van der Waals radii are also included. Symmetry codes: (i) $x-1, y, z$; (ii) $x-1, y-1, z$; (iii) $x+1, y, z$.

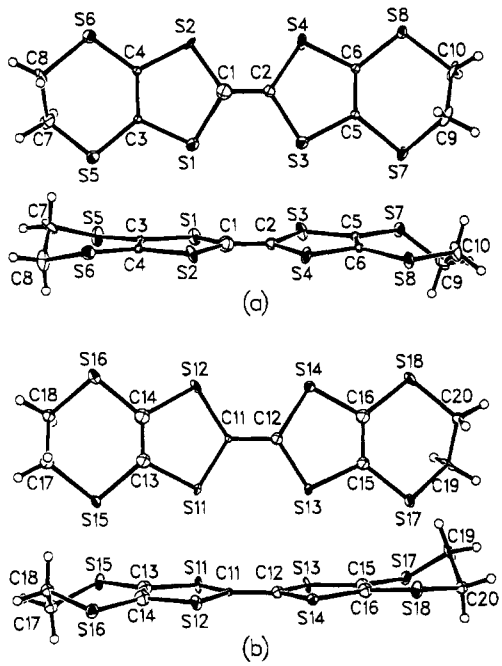

Figure 1. Top and side views of the two crystallographically nonequivalent ET molecules [(a) molecule 1, (b) molecule 2] in $(ET)_2Br_2SeCN$ at 122 K. Thermal ellipsoids are drawn with a 50% probability cutoff.

thermal contraction of the crystal lattice, most of the intermolecular S···S contacts, listed in Table 3, decrease upon cooling. However, the significant change in the unit cell angles between 298 and 122 K causes some twisting of the ET molecules, especially molecule 2 (with atom numbers greater than 10) whose angle of the C=C double bond with the *ab*-plane normal changes by 3°. This twist causes the S5···S13 contact to increase upon cooling.

The overall geometry of the *T*-shaped anion (Figure 3) is similar to that reported for the phenyltrimethylammonium[8] and tetramethylammonium[15] salts. The Se−Br distances are equal the average of those reported. However, the Se−C distance is approximately 0.1 Å shorter and the C−N distance ca. 0.1 Å longer than in the other compounds. These differences can be explained in terms of the *inter*molecular interactions between the p_π orbital of selenium and the π^* orbital of the CN group. The "non"-bonded Se···N contact of 2.95 Å is significantly shorter than in the Ph_3MeN^+ (3.20 Å) and the Me_4N^+ (3.17 Å) salts. All of these contacts are well within the sum of the van der Waals radii (3.45 Å)[16] for the two elements. These intermolecular $p_\pi-\pi^*$ interactions slightly strengthen the Se−C single bond and similarly weaken the C−N triple bond, thus changing the observed bond lengths.

Because of the rather large change in unit cell angles between room temperature and 122 K, the unit cell parameters were determined at a number of temperatures between these extremes, in order to examine if the change was gradual or if a phase transition occurred. A transition was suggested by the anomaly around 150 K in the resistivity data. Unit cell length and volume ratios and angle differences (relative to room temperature) are shown in Figure 4. These values were determined from the setting angles of 21 carefully centered reflections at each temperature (in approximately 10 K intervals). At 153 K, centering was difficult, as the reflections were broader than at the surrounding temperatures, and the lattice parameter least-squares procedure was less accurate. As can be seen, from Figure 4, a phase transition occurs in that temperature range. The *a* and *b* unit cell lengths, as well as the unit cell volume exhibit a step discontinuity, and the angles α and β, which are approximately constant above 160 K, suddenly deviate by almost 2° below 150 K.

Band Electronic Structure. We examined the electronic band structure of $(ET)_2Br_2SeCN$ by performing extended Hückel tight binding (EHTB) calculations[17,18] for a single donor-molecule layer. The calculations were carried out by use of atomic coordinates from both, the room and low temperature structures, with essentially identical results. Figure 5 shows the dispersion relations of the two highest occupied bands of $(ET)_2Br_2SeCN$, which are derived primarily from the HOMO of each donor molecule. The two bands are more dispersive along the a^*- than along the b^*-direction. This reflects the fact that more short intermolecular S···S contacts are present along the *inter*stack than along the *intra*stack direction, and hence the HOMO−HOMO interactions between adjacent donor molecules

(15) Bjørnevåg, S.; Gahre, P. U.; Hauge, S.; Vikane, O. *Acta Chem. Scand.* **1984**, *A38*, 175.

(16) Bondi, A. *J. Phys. Chem.* **1964**, *68*, 441.

(17) Whangbo, M.-H.; Hoffmann, R. *J. Am. Chem. Soc.* **1978**, *100*, 6093.

(18) The atomic orbitals of C, S and Se were represented by double-ζ Slater type orbitals (Whangbo, M.-H.; Williams, J. M.; Leung, P. C. W.; Beno, M. A.; Emge, T. J.; Wang, H. H.; Carlson, K. D.; Crabtree, G. W. *J. Am. Chem. Soc.* **1985**, *107*, 5815), and a modified Wolfsberg−Helmholz formula was used to calculate the off-diagonal H_{ij} values (Ammeter, J. H.; Bürgi, H.-B.; Thibeault, J.; Hoffmann, R. *J. Am. Chem. Soc.* **1978**, *100*, 3686).

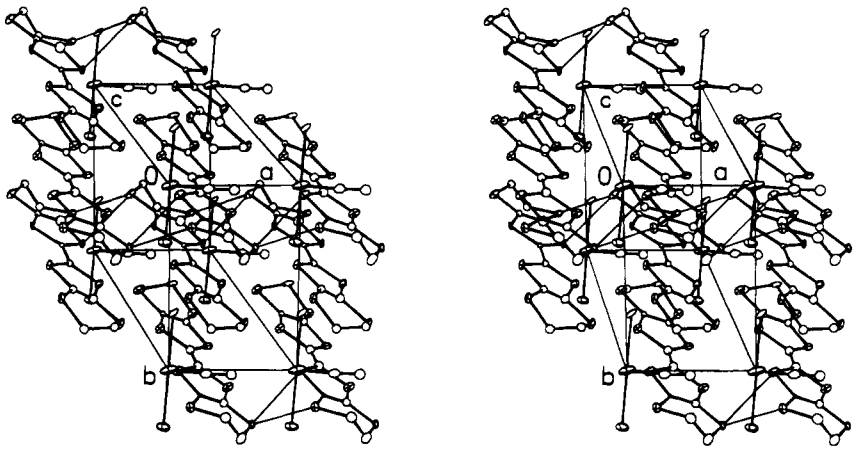

Figure 2. Stereoview of the unit cell and adjacent areas in (ET)$_2$Br$_2$SeCN at 122 K. S···S contacts shorter than 3.6 Å are indicated by thin lines, and hydrogen atoms are omitted for clarity. Thermal ellipsoids are drawn with a 50% probability cutoff.

Table 4. Interatomic angles (deg) in (ET)$_2$Br$_2$SeCN

	T = 298 K	T = 122 K		T = 298 K	T = 122 K
C0–Se–Br1	88.4(3)	89.1(2)	C9A–C10A–S8	117.0(20)	116.2(9)
C0–Se–Br2	91.2(3)	90.8(2)	C9B–C10B–S8	102.1(13)	
Br1–Se–Br2	179.20(13)	179.85(14)	C11–S11–C13	93.9(7)	94.0(6)
N–C0–Se	168.7(10)	177.0(6)	C11–S12–C14	93.8(7)	92.3(5)
C1–S1–C3	96.4(7)	96.3(6)	C12–S13–C15	96.9(7)	94.0(6)
C1–S2–C4	97.0(7)	98.5(6)	C12–S14–C16	97.7(7)	95.0(5)
C2–S3–C5	94.2(6)	97.5(5)	C13–S15–C17A	112.7(13)	99.2(6)
C2–S4–C6	93.3(7)	95.7(6)	C13–S15–C17B	103.7(8)	
C3–S5–C7A	96.0(7)	101.9(5)	C14–S16–C18	101.3(9)	100.3(6)
C3–S5–C7B	99.7(8)		C15–S17–C19	105.4(9)	97.3(6)
C4–S6–C8A	107.3(9)	101.4(6)	C16–S18–C20A	100.4(9)	103.1(6)
C4–S6–C8B	99.7(8)		C16–S18–C20B	99.1(8)	
C5–S7–C9A	95.0(8)	99.7(5)	C12–C11–S11	126.8(12)	122.8(8)
C5–S7–C9B	100.5(8)		C12–C11–S12	118.5(13)	120.5(8)
C6–S8–C10A	107.3(11)	101.6(6)	S11–C11–S12	114.6(7)	116.7(7)
C6–S8–C10B	100.2(8)		C11–C12–S13	118.2(13)	119.7(7)
C2–C1–S1	118.4(10)	120.4(10)	C11–C12–S14	129.4(13)	123.8(8)
C2–C1–S2	125.7(10)	125.5(10)	S13–C12–S14	112.4(9)	116.3(6)
S1–C1–S2	115.8(8)	114.1(7)	C14–C13–S11	121.6(13)	117.3(10)
C1–C2–S3	124.7(9)	123.6(10)	C14–C13–S15	127.3(13)	130.8(10)
C1–C2–S4	119.0(9)	122.9(10)	S11–C13–S15	111.1(9)	111.6(7)
S3–C2–S4	116.2(6)	113.4(7)	C13–C14–S12	116.0(12)	119.4(10)
C4–C3–S1	114.3(10)	116.6(8)	C13–C14–S16	133.4(12)	129.7(10)
C4–C3–S5	129.1(11)	127.3(8)	S12–C14–S16	110.5(7)	110.8(5)
S1–C3–S5	116.5(8)	115.9(6)	C16–C15–S13	114.7(10)	117.5(10)
C3–C4–S2	116.3(10)	114.5(8)	C16–C15–S17	129.7(12)	129.2(10)
C3–C4–S6	124.1(11)	126.9(8)	S13–C15–S17	115.5(8)	113.2(7)
S2–C4–S6	119.3(8)	118.0(6)	C15–C16–S14	118.2(11)	117.2(10)
C6–C5–S3	119.1(11)	116.1(8)	C15–C16–S18	126.1(11)	127.4(10)
C6–C5–S7	129.2(11)	127.6(8)	S14–C16–S18	115.5(8)	115.3(7)
S3–C5–S7	111.6(8)	116.2(5)	C18–C17A–S15	113.6(19)	117.9(9)
C5–C6–S4	116.9(12)	117.1(9)	C18–C17B–S15	117.4(16)	
C5–C6–S8	128.9(11)	130.3(10)	C17A–C18–S16	130.7(16)	116.8(10)
S4–C6–S8	114.1(9)	112.5(7)	C17B–C18–S16	124.9(16)	
C8A–C7A–S5	108.5(12)	109.7(8)	C20A–C19–S17	122.4(17)	112.4(10)
C8B–C7B–S5	122.5(18)		C20B–C19–S17	113.6(15)	
C7A–C8A–S6	108.0(13)	111.5(8)	C19–C20A–S18	134.5(19)	111.9(9)
C7B–C8B–S6	119.1(17)		C19–C20B–S18	121.5(17)	
C10A–C9A–S7	121.3(17)	113.2(10)			
C10B–C9B–S7	113.4(12)				

are stronger along the interstack direction. According to the widths of the two bands along the a^*- and b^*-directions, the HOMO–HOMO interaction is stronger along the a^*-direction by a factor of seven.

Physical Measurements. The four-probe conductivity (along the largest crystal dimension, usually the a-axis) of (ET)$_2$Br$_2$SeCN showed semiconducting behavior in all samples, see Figure 6. Variations in the exact shape of the resistivity curves can be attributed to the difficulty of attaching leads to the small crystals. Near the crystallographic phase transition, around 150 K, artifacts of the resistivity can be attributed to abrupt changes in the contact resistances due to the shear transformation that occurs in the crystal. A similar discontinuity in the resistivity at 76 K did not correlate with any other measurements and is probably an artifact of the measurement, perhaps caused by condensing residual nitrogen in the sample compartment. Several crystals were examined for possible superconductivity in the ac susceptometer at ambient pressure. No traces of superconductivity were found to temperatures as low as 4.2 K. Even at hydrostatic pressures of 1, 3, and 5 kbar superconductivity was not detected by use of the rf impedance method to temperatures as low as 1.2 K.[13]

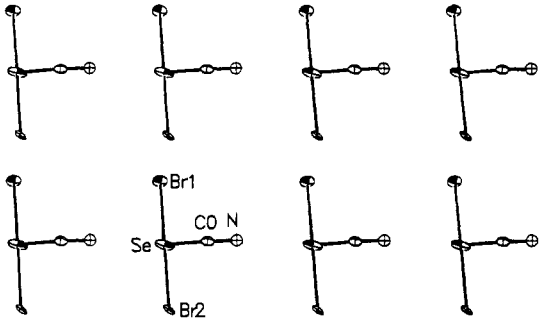

Figure 3. Packing and atomic labeling of the anion layer in $(ET)_2Br_2SeCN$ at 122 K. Thermal ellipsoids are drawn with a 50% probability cutoff.

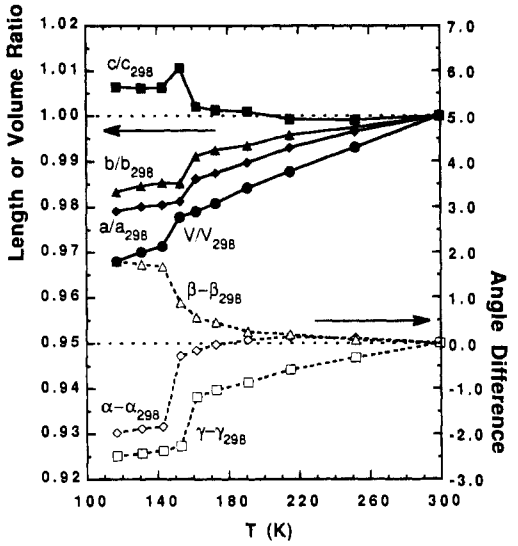

Figure 4. Temperature dependence of the unit cell parameters of $(ET)_2Br_2SeCN$. The axis lengths and the volume are represented as ratios relative to the corresponding room temperature values, whereas the angles are given as differences from their values at 298 K. Note the pronounced discontinuity around 150 K.

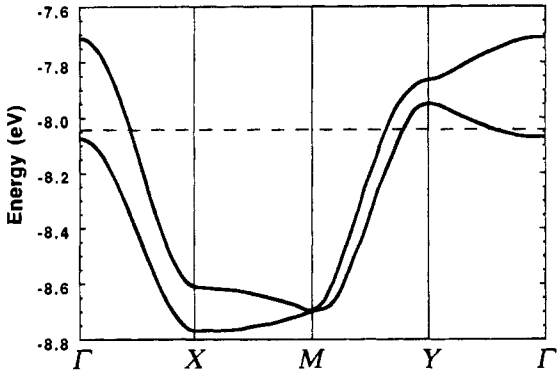

Figure 5. Two-dimensional band electronic structure at 122 K in $(ET)_2Br_2SeCN$. The Fermi level is indicated by a dashed line. The special points in the two-dimensional Brillouin zone are defined as follows: $\Gamma = (0, 0)$, $X = (a^*/2, 0)$, $Y = (0, b^*/2)$, and $M = (a^*2, b^*/2)$.

Two sets of ESR studies were carried out. In the first, a flat, needle-shaped crystal of $(ET)_2Br_2SeCN$ was oriented in the cavity at room temperature in such a way that it could be rotated around its long axis (corresponding to the a-axis, thus the field was rotated in the b^*c^*-plane). 90° corresponded to the field direction along c^*, the normal to the conducting ab-planes, whereas 0° was within the plane (near the b-axis). The peak-to-peak line widths (triangles) and g values (squares) as a function of the rotation angle are plotted in Figure 7. The

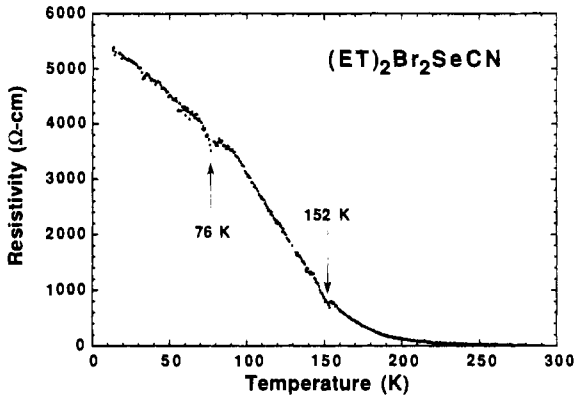

Figure 6. Four-probe electrical resistivity of a single crystal of $(ET)_2Br_2SeCN$ as a function of temperature. See text for a discussion of the features at 152 K and 76 K.

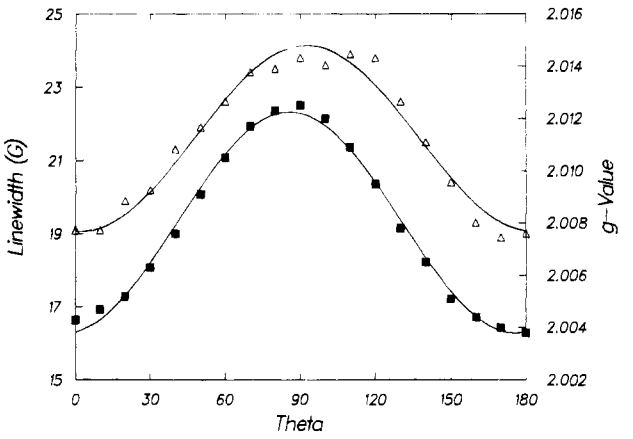

Figure 7. Angle dependence of the g value and the peak-to-peak ESR line width of $(ET)_2Br_2SeCN$ at 298 K. Here 0° corresponds to the magnetic field inside the conducting ab-plane, whereas at 90° the field is perpendicular to the plane.

observed line widths between 19 and 24 G are typical of the β-type packing motif common to $(ET)_2X$ materials.[1] The maximum g value (2.012) occurs at the same angle as the maximum line width, near 90°, where the static magnetic field is approximately parallel to the long molecular axis (central C=C double bond). This behavior is consistent with the reported ESR results for other β-type $(ET)_2X$ salts.[19]

The second ESR experiment was a variable temperature study between 297 and 4 K with the same $(ET)_2Br_2SeCN$ crystal oriented at the 90° angle. The temperature dependence of the peak-to-peak line widths, and the relative spin susceptibilities (squares), are plotted in Figure 8. Between 297 and 160 K, the line width decreased slightly to a local minimum value of 20.5 G at 240 K and then increased to ~23 G at 160 K. Below 160 K, a monotonic decrease in line width with decreasing temperature was observed. The spin susceptibility (proportional to the integrated peak area) approximately followed these changes. Between 297 and 240 K, the relative spin susceptibility increased very slightly. The behavior was consistent with a paramagnetic system containing isolated spins. Below 240 K, the relative spin susceptibility dropped by approximately 75% from 1.04 to 0.27 (relative to 297 K) at 4 K with a small local maximum around 160 K. The anomaly near 160 K in both the line width and the spin susceptibility is likely associated with the structural phase transition, as reported in the structure section. The strong decrease in spin susceptibility below 240

(19) Sugano, T; Saito, G.; Kinoshita, M. *Phys. Rev. B: Condens. Matter* **1987**, *35*, 6554.

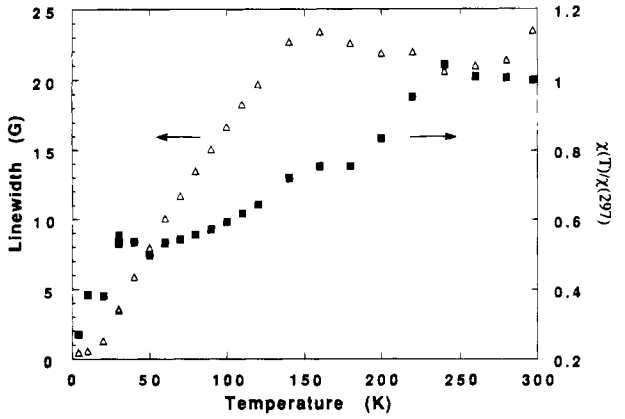

Figure 8. Temperature dependence of the ESR line width and the magnetic spin susceptibility (obtained by integration of the ESR signal) of a single crystal of (ET)$_2$Br$_2$SeCN with the magnetic field oriented perpendicular to the donor molecular *ab*-layer.

K indicated that the unpaired spins were pairing up and the ground state of the title compound was a diamagnetic insulator.

Discussion

The synthesis of the title salt, (ET)$_2$Br$_2$SeCN, did not follow the usual route, i.e., its electrocrystallization could not be accomplished by the use of an electrolyte solution containing the desired anion in the form of a soluble salt with a large counter-cation, as is the usual procedure for the synthesis of ET-based cation-radical salts.[1] The Br_2SeCN^- anion is too strong an oxidant for this method to work. When a solution of (PhMe$_3$N)Br$_2$SeCN is combined with one of ET in 9:1 (v/v) TCE/ethanol, a dark precipitate immediately forms, which has been identified by elemental analysis to be of the same composition as the title salt, but a different crystallographic modification, since its powder diffraction pattern does not match that of the title compound. The precipitation reaction is assumed to follow the overall reaction scheme

$$4ET + 3Br_2SeCN^- \rightarrow 2(ET)_2Br_2SeCN + SeCN^- + 2Br^-$$

Electrocrystallization of single crystals of (ET)$_2$Br$_2$SeCN was achieved by the use of (PhMe$_3$N)SeCN and CuBr as electrolytes. The formation of the Br_2SeCN^- anion presumably occurs near the cathode surface where Cu^+ is reduced, plating the platinum electrode visibly with elemental copper. That the copper ions in CuBr are involved in the formation of Br_2SeCN^- was shown by futile attempts to crystallize (ET)$_2$Br$_2$SeCN from electrolyte solutions containing $SeCN^-$ and alternate sources of bromide ion (i.e., tetrabutylammonium bromide or potassium bromide with 18-crown-6 to enhance solubility). None of these electrolytes produced crystals during electrocrystallization attempts. We propose the following sequence of reactions, involving the stepwise addition of CuBr to the selenium end of $SeCN^-$ and the elimination of elemental copper upon formation of Se−Br bonds:

$$CuBr \xrightarrow{+SeCN^-} [BrCuSeCN^-] \xrightarrow[-Cu]{} [BrSeCN^-] \xrightarrow{+CuBr}$$

$$[BrCuSe(Br)CN^-] \xrightarrow[-Cu]{} Br_2SeCN^-$$

The crystallization of (ET)$_2$Br$_2$SeCN begins no less than 2 weeks after electrolysis commences, with the actual crystal growth occurring on the glass walls of the H-cells, unlike most cation-radical salts which form on the anode itself. As was found when solutions of ET and Br_2SeCN^- were mixed together, the anion is a strong enough oxidant to react with ET, and crystals form whenever the product of the above reaction, which occurs primarily in the cathode compartment of the cell, reaches the ET solution in the anode compartment by slow diffusion through the separating glass frit. The kinetic conditions apparently determine which crystallographic modification of (ET)$_2$Br$_2$SeCN is formed.

Band electronic structure calculations have been extremely useful for the description of the electrical properties of organic charge transfer salts.[20] In the present compound, there are two donor molecules per unit cell in a donor-molecule layer so that, with the oxidation state $(ET)_2^+$, there are three electrons to fill the two bands shown in Figure 5. The dashed line in that figure is the Fermi level appropriate for the case when all the levels below it are doubly occupied. This picture is valid for a normal metallic state in which electron−electron repulsion is small compared with the widths of the partially filled bands.[21-23] However, a metallic picture is not relevant for (ET)$_2$Br$_2$SeCN, because its resistance vs temperature behavior indicates activated transport. Electron localization in a system with partially filled bands can be induced either by electron−electron repulsion[21-23] or by random potentials.[24,25] Electron−electron repulsion can induce a state in which an odd electron is localized in every $(ET)_2^+$ dimer unit. Alternatively, one might consider that electron localization in (ET)$_2$Br$_2$SeCN originates from the random potentials associated with crystallographic disorder in the ethylene group positions of ET. However, the ethylene group positions are ordered at 122 K, but (ET)$_2$Br$_2$SeCN is not metallic below 122 K. Thus, it appears that the localized state in which an odd electron is localized in every $(ET)_2^+$ dimer unit is more consistent with the resistivity behavior of (ET)$_2$Br$_2$SeCN. This observation, together with the fact that the donor−donor interaction is stronger along the a^*- than in the b^*-direction by a factor of 7, suggests that the magnetic susceptibility of (ET)$_2$Br$_2$SeCN will exhibit a strong anisotropy.

Acknowledgment. Work at Argonne National Laboratory and Sandia National Laboratories is sponsored by the U.S. Department of Energy, Office of Basic Energy Sciences, Division of Materials Sciences, under Contracts W-31-109-Eng-38 and DE-AC04-94AL85000, respectively. J.L.S., A.C.C., and M.C. are Student Undergraduate Research Participants from Western Montana College, Dillon, MT, Alma College, Alma, MI, and Wagner College, Staten Island, NY, respectively, sponsored by the Argonne Division of Educational Programs. Work at North Carolina State University is supported by the U.S. Department of Energy, Office of Basic Sciences, Division of Materials Sciences, under Grant DE-FG05-86ER45259.

Supplementary Material Available: Tables giving crystal data and experimental detals of the X-ray diffraction data collection, and anisotropic thermal parameters (5 pages). Details are given on any current masthead page.

(20) Whangbo, M.-H.; Williams, J. M.; Leung, P. C. W.; Beno, M. A.; Emge, T. J.; Wang, H. H.; Carlson, K. D.; Crabtree, G. W. *J. Am. Chem. Soc.* **1985**, *107*, 5815.
(21) Mott, N. F. *Metal-Insulator Transitions*; Barnes and Noble: New York, 1977.
(22) Brandow, B. H. *Adv. Phys.* **1977**, *26*, 651.
(23) Whangbo, M.-H. *J. Chem. Phys.* **1979**, *70*, 4963.
(24) Anderson, P. W. *Phys. Rev.* **1958**, *109*, 1492.
(25) Hayes, W.; Stoneham, A. M. *Defects and Defect Processes in Nonmetallic Solids*; Wiley: New York, 1985; Chapter 8.